

The link between galactic satellite orbits and subhalo accretion

Mark R. Lovell¹, Vincent R. Eke¹, Carlos S. Frenk¹, and Adrian Jenkins¹

¹*Institute for Computational Cosmology, Durham University, South Road, Durham, DH1 3LE*

Accepted 2011 January 17. Received 2010 December 9; in original form 2010 July 28

ABSTRACT

We calculate the orbital angular momentum of dark matter subhaloes in the Aquarius simulations of cold dark matter (CDM) galactic haloes. We calculate the orientation of their angular momentum relative to that of the spin vector of their host halo and find a variety of different configurations. All six Aquarius haloes contain statistically significant populations of subhalo orbits that are aligned with the main halo spin. All haloes possess a population of subhaloes that rotates in the same direction as the main halo and three of them possess, in addition, a population that rotates in the opposite direction. These configurations arise from the filamentary accretion of subhaloes. Quasi-planar distributions of coherently rotating satellites, such as those inferred in the Milky Way and other galaxies, arise naturally in simulations of a Λ CDM universe.

Key words: galaxies: formation - dark matter

1 INTRODUCTION

It has been known for several decades that the 11 ‘classical’ satellites of the Milky Way define a thin plane around the Galaxy (Lynden-Bell 1976). Some of the faint satellites recently discovered in the Sloan Digital Sky Survey (SDSS; York et al. 2000; Willman et al. 2005a,b; Sakamoto & Hasegawa 2006; Zucker et al. 2006a,b; Irwin et al. 2007; Walsh et al. 2007; Belokurov et al. 2008) also appear to have an anisotropic distribution reminiscent of that of the classical 11 (Metz et al. 2009). The presence of such a ‘disc-of-satellites’ suggests a common plane of rotation in the Milky Way. Measurements of proper motions, which are now possible for some of the satellites, can be used to constrain the nature of any systemic rotation (Metz et al. 2008; Lux et al. 2010).

In tandem with these observational developments, advances in computational cosmology now make it possible to simulate galactic haloes with sufficient resolution to probe the properties of satellites and investigate the origin of their flattened configuration. N-body simulations from cold dark matter (CDM) initial conditions show that a large number of accreted haloes survive to the present, making up a population of ‘subhaloes’ of the ‘main halo,’ some of which could host the satellites.

The observations, however, suggest a complex formation history. First, the number of satellites identified so far is much smaller than the number of dark subhaloes in the simulations, giving rise to the so-called ‘missing satellite problem’ (Moore et al. 1999; Klypin et al. 1999). Secondly, the

thin ring around the sky delineated by the classical satellites contrasts with the distribution of subhaloes in the simulations which is triaxial (Libeskind et al. 2005; Zentner et al. 2005). Thirdly, the inferred angular momentum vectors of the majority of the classical satellites in the Milky Way point towards a patch on the sky of diameter no greater than 30° , which has led Metz et al. (2008, 2009) to argue that the observed satellites cannot have formed in cold dark matter subhaloes. In contrast to the Milky Way, NGC 5084 appears to have a population of satellites orbiting in the opposite sense to the galaxy (Carignan et al. 1997).

The combination of ‘missing satellites’, an anisotropic distribution and coherent orbits is sometimes viewed as a challenge to the CDM model (e.g. Moore et al. 1999; Metz et al. 2008). However, a number of studies using semi-analytic modelling and hydrodynamic simulations have shown that a relatively small satellite population is a natural outcome of galaxy formation in the CDM cosmology (e.g. Kauffmann et al. 1993; Bullock et al. 2000; Benson et al. 2002; Somerville 2002; Koposov et al. 2009; Muñoz et al. 2009; Busha et al. 2010; Cooper et al. 2010; Li et al. 2010; Macciò et al. 2010; Wadepuhl & Springel 2011). The simulations show that satellites form only in a small fraction of subhaloes which turn out to be those that had the most massive progenitors at the time of accretion (Libeskind et al. 2005). Furthermore, disc-like subhalo configurations are seen to form in Λ CDM cosmological simulations (Kang et al. 2005; Zentner et al. 2005; Libeskind et al. 2007; Li & Helmi 2008; Libeskind et al. 2009). Such systems appear to be related to the preferential accretion of haloes along the fil-

aments of the cosmic web. Haloes tend to fall along the central spines of filaments, so that the range of trajectories, and thus orbits, that they acquire when they enter a halo is restricted (Libeskind et al. 2009).

Shaw et al. (2006), Warnick & Knebe (2006) and Libeskind et al. (2009) confirmed the conclusion of Libeskind et al. (2005) that satellite accretion is a highly anisotropic process and found in their simulations a significant population of subhaloes that co-rotated with the spin of their hosts. However, Shaw et al. (2006) simulated galaxy cluster haloes, not galactic haloes; Warnick & Knebe (2006) also focused on cluster haloes except for one example of a galaxy halo which, however, had only moderate resolution (a minimum subhalo mass of $m_{\min} = 5.7 \times 10^7 M_{\odot}$). The largest sample of galaxy halo simulations so far is that of Libeskind et al. (2009). They analysed 436 haloes but were only able to resolve subhaloes of mass $m_{\min} \geq 2.76 \times 10^9 M_{\odot}$.

In this study, we analyse the state-of-the-art, high resolution simulations of six galactic haloes of mass $\sim 1 \times 10^{12} M_{\odot}$ of the Aquarius project (Springel et al. 2008b). These simulations resolve subhaloes of mass exceeding $\sim 10^5 M_{\odot}$. We calculate the angular momentum of subhaloes, and use the results to interpret the Milky Way data. The paper is organised as follows. In Section 2 we briefly describe the Aquarius project and the analysis performed for this paper. The results follow in Section 3 and our conclusions in Section 4.

2 THE SIMULATIONS

The Aquarius project is a set of dark matter simulations containing haloes similar in size and environment to those of the Milky Way; each one has been run from $z = 127$ to $z = 0$. There are six different haloes (Aq-A - Aq-F), each of which has been resimulated at at least two levels of resolution (L1, the highest, down to L5, the lowest). They were performed using the GADGET-3 code (Springel et al. 2008b). In all cases, the resimulations at different resolutions show remarkable convergence in the positions and internal properties of subhaloes. This project has already yielded several interesting results, including a study of the near-universality of halo density profiles (Springel et al. 2008b; Navarro et al. 2010), predictions for the γ -ray signal from annihilating dark matter in the galactic halo (Springel et al. 2008a) and for direct dark matter detection experiments (Vogelsberger et al. 2009). A summary of key parameter values for each simulation is given in Table 1.

It is important for this study to establish that the sample of six Aquarius haloes can be considered at least approximately representative of the population of Milky-Way mass haloes as a whole. The Aquarius haloes are all drawn from the same parent cosmological simulation, and it is possible to address this issue directly for several properties. The spins, concentrations and formation histories of the Aquarius haloes are compared to the parent population in Boylan-Kolchin et al. (2010). Broadly speaking, the properties of the Aquarius haloes span the expected range for the population as a whole. We give the values of the halo spin, concentration and formation redshift, defined as the redshift when half the halo mass is assembled, in Table 1. Also in the table we list the shape axis ratios for the haloes, approx-

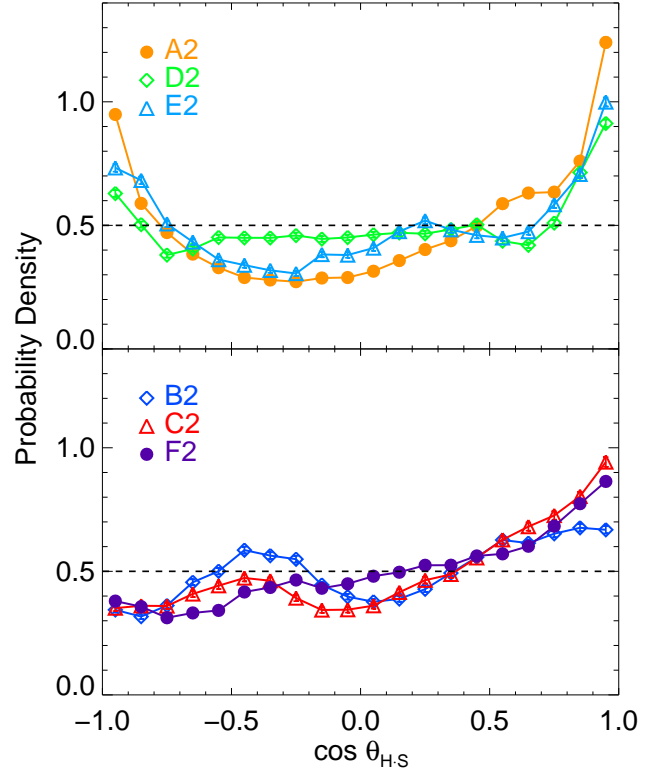


Figure 1. The distribution of $\cos \theta_{H,S}$ for the six Aquarius haloes at resolution level L2, where $\theta_{H,S}$ is the angle between the main halo spin and subhalo orbit vectors. The six are separated into two panels according to whether or not they exhibit an antiparallel tail greater than 0.5. *Top panel:* results for Aq-A2 (orange), Aq-D2 (green), and Aq-E2 (light blue). *Bottom panel:* as above, but for Aq-B2 (blue), Aq-C2 (red), and Aq-F2 (purple). In both cases, the dashed line corresponds to an isotropic distribution.

imating them as ellipsoids. The axis ratios are taken from Vera-Ciro et al. (in preparation) and calculated for ellipsoids which are determined by applying the iterative method of Allgood et al. (2006) to the haloes with the substructure removed (actually to the ‘main halo’, defined below). The six haloes show a range of shapes and are typical for Λ CDM haloes (Allgood et al. 2006; Bett et al. 2007).

The halo membership of each particle is determined using the friends-of-friends (FOF) algorithm (Davis et al. 1985). The particles in each FOF group are, in turn, assigned to self-bound structures using the SUBFIND code (Springel et al. 2001). We call the largest of these self-bound substructures the main halo, and the remainder we call subhaloes. A small proportion (< 1 per cent) of the particles within the FOF group are found to form a ‘fuzz’ that is not gravitationally bound to any other object; they are not considered any further.

Our primary aim is to determine the orientations of dark matter subhalo orbits in the Aquarius simulations and compare the results with data for galactic satellites. We calculate the ‘main halo spin’, defined as the sum of the angular momenta of all main halo particles about their centre-of-mass. For each subhalo, we calculate the ‘subhalo orbital spin’, defined as the vector associated with the angular mo-

Name	m_p [M_\odot]	r_{200} [kpc]	M_{200} [M_\odot]	n_s	λ	c_{NFW}^*	z_{form}	q	p
Aq-A1	1.712×10^3	245.76	2.523×10^{12}	197484	-	16.11	1.93	-	-
Aq-A2	1.370×10^4	245.88	2.524×10^{12}	30177	0.027	16.19	1.93	0.866	0.687
Aq-A3	4.911×10^4	245.64	2.524×10^{12}	9489	-	16.35	1.93	0.862	0.688
Aq-A4	3.929×10^5	245.70	2.524×10^{12}	1411	-	16.21	1.93	0.844	0.700
Aq-A5	3.143×10^6	246.37	2.541×10^{12}	246	-	16.04	1.93	0.830	0.685
Aq-B2	6.447×10^3	187.70	1.045×10^{12}	31050	0.022	9.72	1.39	0.820*	0.839*
Aq-C2	1.399×10^4	242.82	2.248×10^{12}	24628	0.020	15.21	2.23	0.711*	0.770*
Aq-D2	1.397×10^4	242.85	2.519×10^{12}	36006	0.012	9.37	1.51	0.846*	0.901*
Aq-E2	9.593×10^3	212.28	1.548×10^{12}	30372	0.017	8.26	2.26	0.898*	0.674*
Aq-F2	6.776×10^3	209.21	1.517×10^{12}	35041	0.050	9.82	0.55	0.700†	0.866†

Table 1. Selected parameters of the Aquarius simulations used in this paper. The simulation name encodes the halo label (Aq-A, B, and so on) and the numerical resolution level (1 to 5, hereafter L1, L2, L3, L4, L5). m_p is the particle mass, r_{200} the radius of the sphere of density 200 times the critical density, M_{200} the halo mass within r_{200} , n_s the number of subhaloes within the main halo, λ the spin parameter as determined by Boylan-Kolchin et al. (2010), and q, p the halo shape axis ratios b/a and c/b respectively (Vera-Ciro et al., in preparation). The axes are defined as $a \geq b \geq c$ for ellipsoids determined using the method of Allgood et al. (2006). Values with * or † superscripts were calculated for haloes at resolution levels L4 or L3 respectively. As the smallest subhaloes determined by SUBFIND contain 20 particles, the minimum subhalo mass in each simulation is $20m_p$.

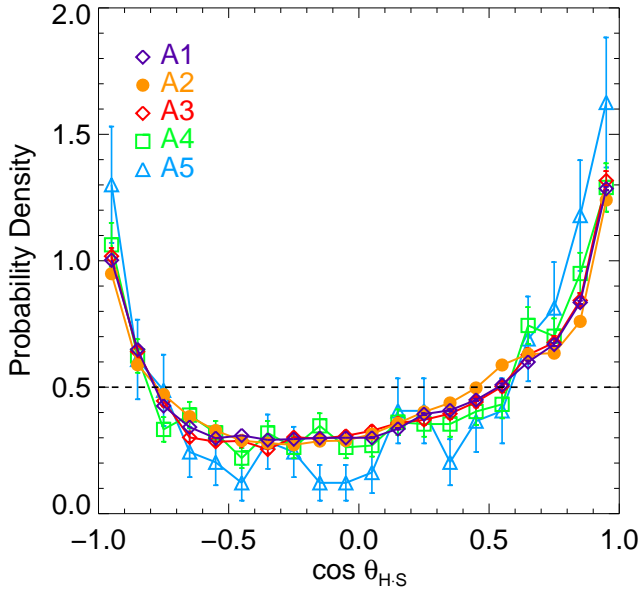


Figure 2. The distribution of $\cos \theta_{\text{H,S}}$ for all the resolution levels of Aq-A. Aq-A1 contains 197484 subhaloes (purple), Aq-A2 30177 (orange), Aq-A3 9489 (red), Aq-A4 1411 (green), and Aq-A5 246 (light blue). The error bars denote Poisson uncertainties.

mentum of each subhalo about the centre of the main halo. We then calculate the cosine of the angle, $\theta_{\text{H,S}}$, between the main halo spin vector and the subhalo orbit vector for every subhalo associated with that main halo. These subhaloes are tracked back to the initial conditions in order to investigate the origin of the patterns that we find.

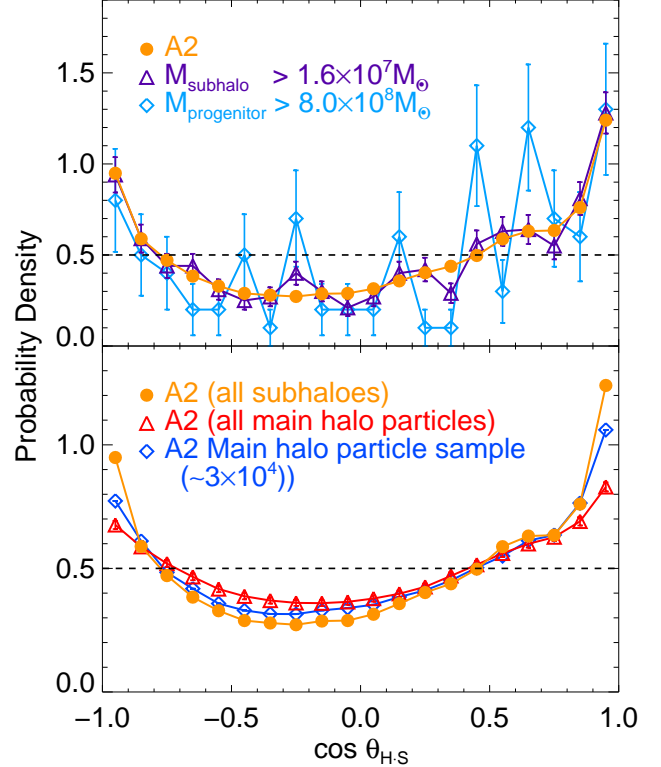


Figure 3. The distribution of $\cos \theta_{\text{H,S}}$ for different populations. *Top panel:* comparison of the 1000 most massive subhaloes at $z = 0$ (purple) with the 100 subhaloes that have the most massive progenitors (light blue), and the entire population of Fig. 2 (orange). *Bottom panel:* comparison of the $\cos \theta_{\text{H,S}}$ distribution for subhaloes with two populations of main halo particles: a sample of 3×10^4 selected to have the same radial distribution as the main halo (blue) and the full population (red).

3 RESULTS

We first describe our calculation of the angular momentum distributions of various populations and then investigate their origin.

3.1 Angular momentum distributions of subhaloes

We compute $\cos \theta_{H,S}$ for each of the six L2 haloes at $z = 0$ as described above, and plot the results in Fig. 1 as a probability density; an isotropic distribution of angular momenta in this plot corresponds to a horizontal line at 0.5.

All the haloes show a statistically significant bias for subhalo orbits to be aligned (parallel) to the rotation of the parent main halo, as found by Shaw et al. (2006) and Warnick & Knebe (2006). The average fraction of corotating subhaloes in the Aquarius haloes is 57 per cent, with a narrow range between 54 per cent and 61 per cent. This is consistent with the average of 59 per cent quoted by Warnick & Knebe (2006). This result is a natural outcome of tidal torque theory (Hoyle 1951; White 1984) when the primordial dark matter protohaloes exert torques on one another, inducing net spins as they condense.

We also find significant numbers of nearly *anti*-parallel orbits in three of our haloes. Specifically, haloes Aq-A2, Aq-D2, and Aq-E2 show a significant proportion of subhalo orbits in the $-1.0 < \cos \theta_{H,S} < -0.9$ bin (9.5 per cent, 6.3 per cent, and 7.3 per cent respectively where 5 per cent would be expected for a random distribution - the Poisson errors on our L2 measurements are negligible), whilst Aq-B2, Aq-C2, and Aq-F2 do not. We have separated the haloes into two panels according to this property. We find an antiparallel excess in three out of six of our haloes, whereas Warnick & Knebe (2006) only have one such halo out of their sample of nine. Adopting the same binning as Warnick & Knebe (2006) does not change our result. With such small halo samples it is unclear whether this particular result is consistent or inconsistent between the two studies.

To test if our results are robust to changes in resolution, we repeat this calculation for the five different resolution levels of the Aq-A halo (Fig. 2). We see that Aq-A1 together with Aq-A3, Aq-A4, and Aq-A5 has an angular momentum distribution broadly of the same form as Aq-A2, with increasing noise as the resolution decreases because of the smaller number of subhaloes. Each resolution level is dominated by a different subhalo mass; the minimum subhalo mass in Aq-A5 is $\sim 10^7 M_\odot$, while in Aq-A1 it is three orders of magnitude smaller. We find a similar degree of convergence with numerical resolution for haloes Aq-B through to Aq-F.

In Fig. 3 we probe the orientation of the angular momentum vector of different populations. In the top panel, we compare the distribution for the 1000 largest subhaloes at the final redshift (particle number > 1222 , equivalent to subhalo mass of $1.7 \times 10^7 M_\odot$) with that the 100 subhaloes present at $z = 0$ that had the most massive progenitors and that of the entire halo population. The most massive progenitor is defined as the SUBFIND halo in the merger tree that contained the largest number of particles over the entire history of the simulation. This mass is very close to the mass that the subhalo had at the time it fell into the main halo. It is these subhaloes that are most likely to host

satellite galaxies, according to Libeskind et al. (2009). Of the subhaloes that had the 100 largest progenitors, all but 6 are among the top 1000 most massive subhaloes at redshift zero. The distributions of $\cos \theta_{H,S}$ for all three populations of subhaloes are consistent within the errors.

To establish whether the angular momentum orientation of the subhalo population is special, in the lower panel of Fig. 3 we compare subhaloes in Aq-A2 with particles from the main halo. We create a special sample of halo particles with the same radial distribution as the subhaloes. This is made by first defining a set of about 30 radial bins between the halo centre and the virial radius. The halo subsample is produced by first noting how many subhaloes lie in a particular bin, and then randomly selecting the same number of halo particles from the that same bin. This is always possible as the number of halo particles in any bin exceeds the corresponding number of subhaloes. We compare this particle sample's distribution of $\cos \theta_{H,S}$ with that for the Aq-A2 subhaloes and for the entire set of main halo particles. The three distributions are statistically inconsistent with each other. The subhalo population has a larger fraction of aligned and antialigned members, with the radially selected subsample being intermediate between the subhaloes and the halo particles as a whole. Although even the latter has a non-uniform distribution of angular momenta cosines, it is significantly flatter than that of other two populations. This suggests that the accretion mechanism that supplies subhaloes (of all masses) is somewhat different from the mechanism by which halo particles are accreted, or that the evolution of subhaloes differs from that of halo particles.

To investigate the orientation of the orbital spins in more detail, we plot the angular momentum vectors of each subhalo on an all-sky Mollweide projection, one for each halo at resolution L2. Each map displayed here was divided into ~ 45000 pixels, with angular width $\sim 1^\circ$, and smoothed with a Gaussian beam of FWHM 10° using Healpix routines (Górski et al. 2005). We identify the pixel with the highest density after smoothing, and call this the 'densest point vector'. The pre-smoothing maps for all six L2 haloes are displayed in Fig 4. The main halo spin vector is marked in red, its antipole in blue, and the densest point vector in green.

Aq-A2 exhibits the cleanest structure of all the haloes, with strong clustering around the pole and antipole, joined by two strands. Aq-B2 is, in contrast, characterised by irregular structures concentrated around regions distant from the main halo spin poles. All of the other haloes exhibit clustering around the main halo spin, with other, local, features apparent. The densest point vector position is always closer to the main halo spin than to its antipole. One may think of Figs. 1 to 3 as an integration around lines of equal angle from the red and blue circles. As noted above, we are particularly interested in those subhaloes that are most likely to host satellites, and so we repeat this plot for the 100 subhaloes with largest progenitors in Fig. 5.

As expected from Fig. 3, the 100 subhaloes with the largest progenitors trace the underlying structure of subhaloes in the map traced in Fig. 4. A few of them lie in regions where there are few subhaloes of any mass, and so we might expect to find satellite galaxies spatially removed from the disc-of-satellites for at least some portions of their orbits. The majority, however, lie within underlying struc-

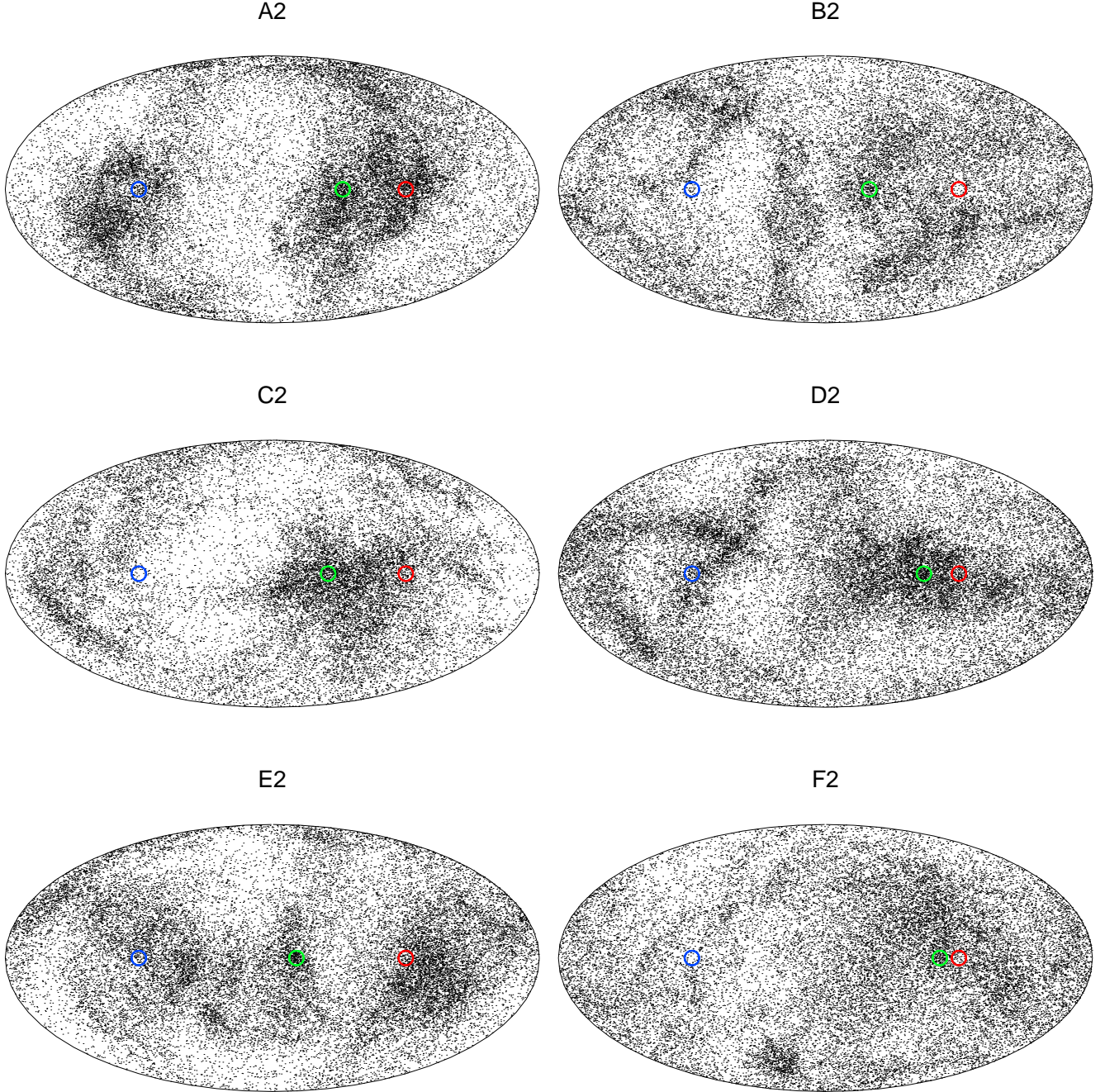


Figure 4. Mollweide projections of the directions of the angular momentum vectors of all subhaloes in the L2 simulations. The red circle shows the direction of the main halo spin, blue the main halo spin antipole, and green the densest collection of vectors after smoothing. The maps have been rotated such that all three circles lie on the equator, with the main halo spin and its antipole lying 90° either side of the centre and the green circle in between. Thus, a subhalo of $\theta_{H,S} = 0^\circ$ will map to the red circle, and one of $\theta_{H,S} = 90^\circ$ to either the plot boundary or a point on the north-south bisector.

tures. The subhaloes with the top 11 progenitors cluster in the same way as the rest of the top 100. Thus, we conclude that observed satellite galaxies should also exhibit coherent motion.

3.2 The origin of coherent rotation

The importance of filamentary accretion can be appreciated by examining the positions of the subhaloes at different snapshots in the simulation. In Fig. 6 we plot the positions of all the subhaloes present at $z = 0$, relative to the centre of the main halo in two projections. On the left, the main halo angular momentum vector points along the positive X-

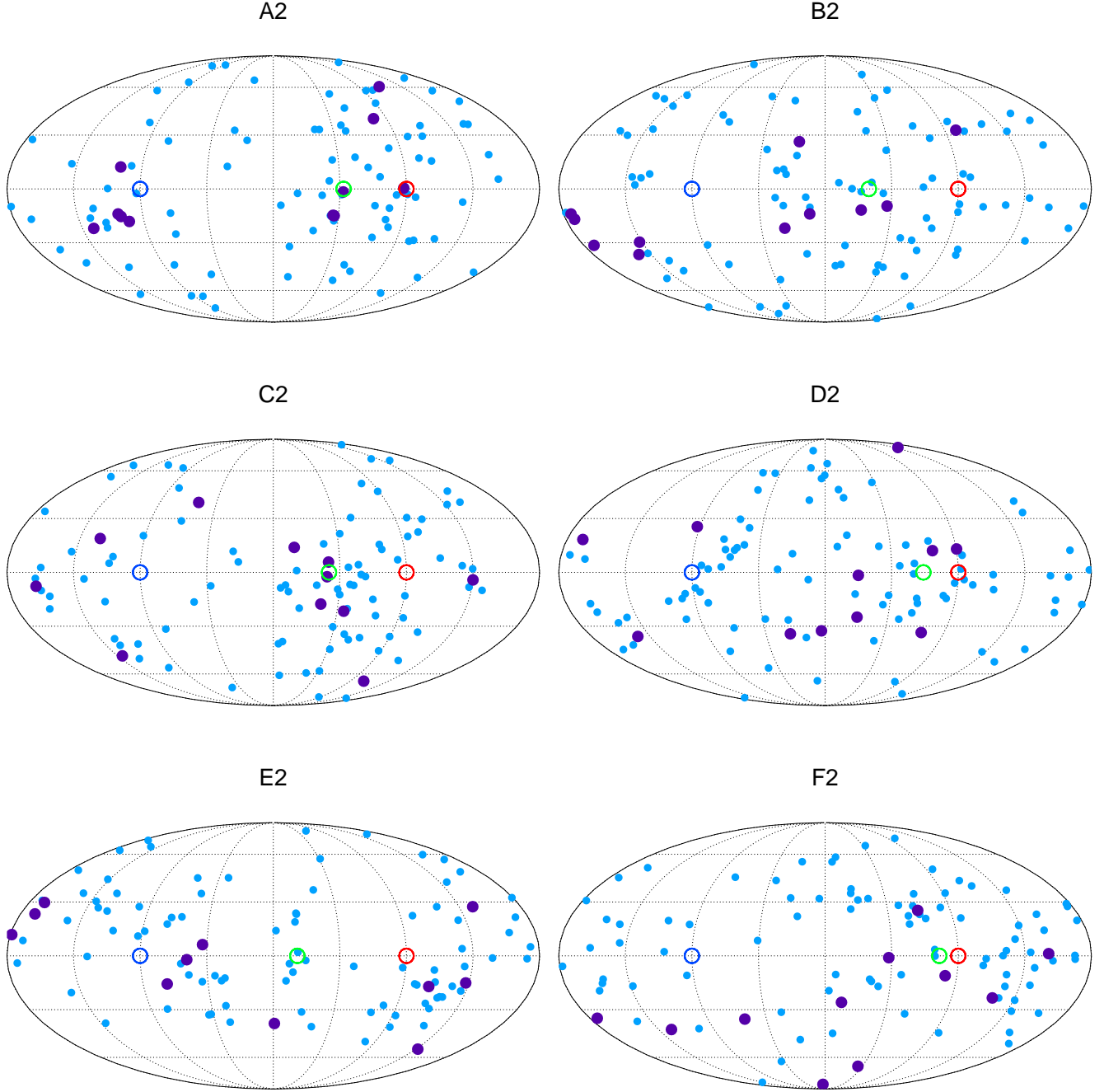


Figure 5. Mollweide projections of the directions of the angular momentum vectors of subhaloes with the largest progenitors in the L2 simulations. Subhaloes with top 100 progenitors are denoted in blue; the subset with the 11 largest progenitors are plotted in purple.

axis, so that the subhalo populations that have $\cos \theta_{H-S} > 0.9$ (red) and $\cos \theta_{H-S} < -0.9$ (blue) appear as an edge-on thick disc. On the right, the angular momentum vector points out of the plane of the page.

In Fig. 7 we investigate the origins of the different populations of subhaloes by plotting their positions in the initial conditions. No subhaloes have condensed at this early time, so we define the ‘position’ of each subhalo as the centre-of-mass of all the particles that will be members of that subhalo at redshift zero. Plotting the position of the most-bound

particle rather than the centre-of-mass makes no difference to the appearance of the plot, and the plotting procedure followed is exactly the same as that used for Fig. 6.

All of the haloes that have an excess of near-antiparallel subhaloes in Fig. 1 show a delineation in the positions of the different subhalo populations. There is also a degree of segregation in Aq-C2, however we find no clear delineation for haloes Aq-B2 and Aq-F2. We can observe how these segregated initial positions evolve into the orbital configurations at the final time by examining snapshots of intermediate

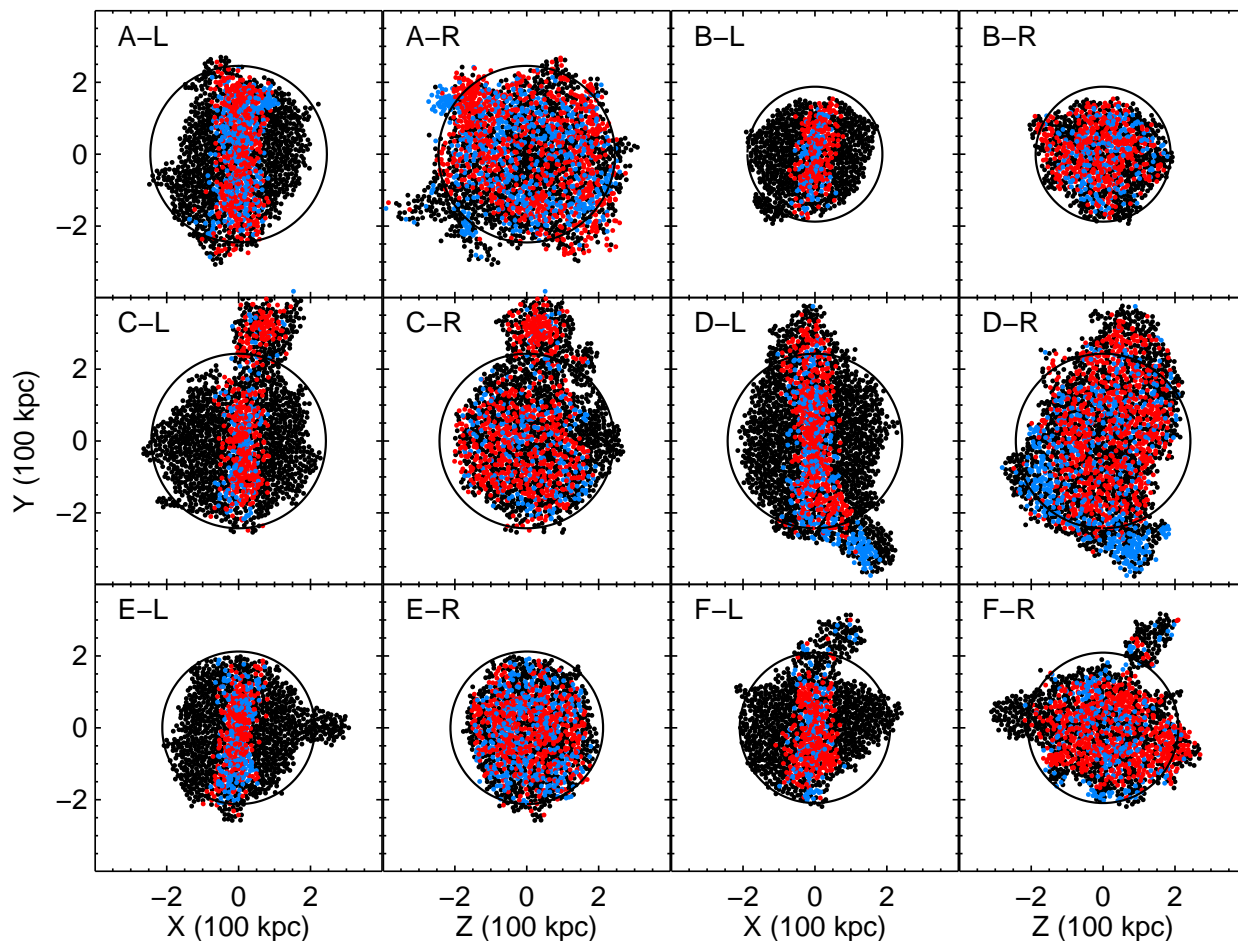


Figure 6. $X - Y$ positions for subhaloes at $z = 0$ in two projections. Subhaloes with $\cos \theta_{H,S} > 0.9$ are indicated in red and those with $\cos \theta_{H,S} < -0.9$ in blue. All other subhaloes are shown in black. The black circle marks the virial radius, r_{200} . *Left panels (i.e. L):* the X axis points in the direction of the main halo spin, so those subhaloes with orbit vectors parallel and antiparallel to the main halo spin appear as a band parallel to the Y axis. *Right Panel (R):* looking down the X axis, so the main halo is spinning anticlockwise. The red and blue points are plotted in a random order on top of the black.

redshift. In the cases of haloes Aq-A and Aq-D, we find that, independent of resolution, the motion of interest of these delineated subhaloes occurs within the plane of the main halo spin (the panels A-R and D-R). This enables us to describe this motion simply with the schematic arrows shown in these panels in Fig. 7. In both of these haloes the near-parallel and near-antiparallel populations collapse to form filaments in their segregated regions. Crucially these filaments are not straight, and the subhaloes follow curved paths into the main halo as shown by their same-colour arrows. ‘Red’ (near-parallel) subhaloes will therefore enter the virial radius with an anti-clockwise orbit around the plot centre, whereas the ‘blue’ will adopt a clockwise orbit. In Aq-D the ‘red’ and ‘blue’ filaments are separate entities, but in Aq-A they lie very close together and give the appearance of one filament fed at each end by two ‘strands’. One of these strands then supplies the near-parallel subhaloes and the other the near-antiparallel.

Aq-E near-antiparallel subhaloes are also accreted through a pair of curved filaments approximately in the plane of the final main halo spin, and so we illustrate the motion of these subhaloes with arrows in Fig. 7 panel E-R. By contrast, the accretion of the red subhaloes is more complex and involves motion at a significant angle to the plane of the main halo spin, and for this reason we do not draw the corresponding red arrows. In Aq-C some of the ‘red’ subhaloes do accrete in a filament, but a large proportion end up in the large lump visible at the top of Fig. 6 panels C-L and C-R. No coherent inflow pattern is apparent for the small population of ‘blue’ subhaloes.

We can describe the accretion geometry further by determining where each subhalo enters the main halo. We find the redshift at which each subhalo attains its highest mass (taken to indicate the time when it falls into the virial radius of the main halo) and thus determine its infall position relative to the main halo centre. The results are plotted in

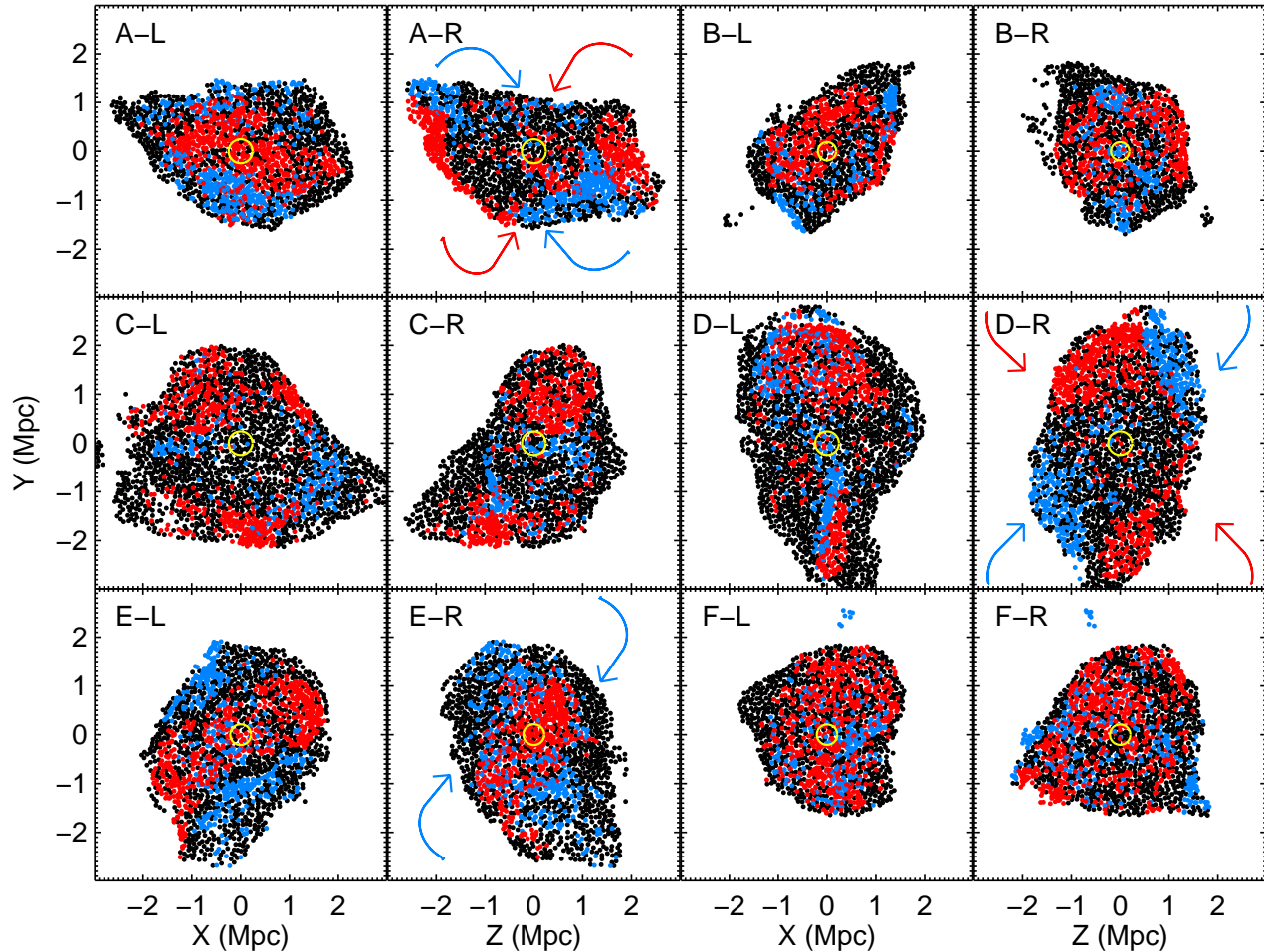


Figure 7. $X - Y$ comoving positions at $z = 127$ of the centre of mass of the particles that end up in each subhalo at $z = 0$. The coordinates are as in Fig. 6, with the main halo spin at $z = 0$ still determining the projections. The final virial radius is indicated in yellow. As stated in the text, the haloes Aq-A2 and Aq-D2 are found to accrete their ‘red’ and ‘blue’ subhaloes in the plane of the main halo spin, and so we have added coloured arrows to the A-R and D-R panels to illustrate schematically the accretion paths for the different subhalo populations. The ‘blue’ subhaloes of Aq-E2 exhibit similar behaviour, and so we have also included arrows to indicate their motion in E-R.

Fig. 8, which is oriented such that the main halo spin points towards the north pole of each projection. We can see that, independent of resolution, the subhalo populations that end up in parallel and antiparallel spin orbits in Aq-A, Aq-D, and Aq-E originate from preferential directions as expected from our visual examination. A majority of subhaloes in Aq-D and Aq-A accrete close to the equator, also as expected, whilst Aq-E acquires a significant proportion of its parallel orbit subhaloes from a patch of sky close to the main halo pole. Any demarcation for haloes Aq-B, Aq-C, and Aq-F is less clear, suggesting that filaments played a lesser role in their accretion history.

4 CONCLUSIONS

In this paper we have characterized the distribution of subhalo orbits in the Aquarius simulations of CDM galactic

haloes and attempted to explain the mechanisms that give rise to them. We find that the complex accretion patterns that build up a halo result in different configurations of subhalo orbits, none of which is close to isotropic. Some are structured in a symmetric way (Aq-A) relative to the spin poles, while others show no strong pattern (Aq-B). In all six haloes we find a large subhalo population that has coherent rotation aligned with the spin of the main halo, in agreement with the results of Libeskind et al. (2009). In three cases there is, in addition, a subhalo population that counter-rotates relative to the main halo. We trace this rather unexpected arrangement back to the filamentary nature of subhalo accretion. If galaxies tend to rotate in the same direction as their parent halo (Bailin et al. 2005; Bailin & Steinmetz 2005; Bett et al. 2010), our results show that it is possible to generate populations of retrograde satellites. Such a population of retrograde satellites appears to

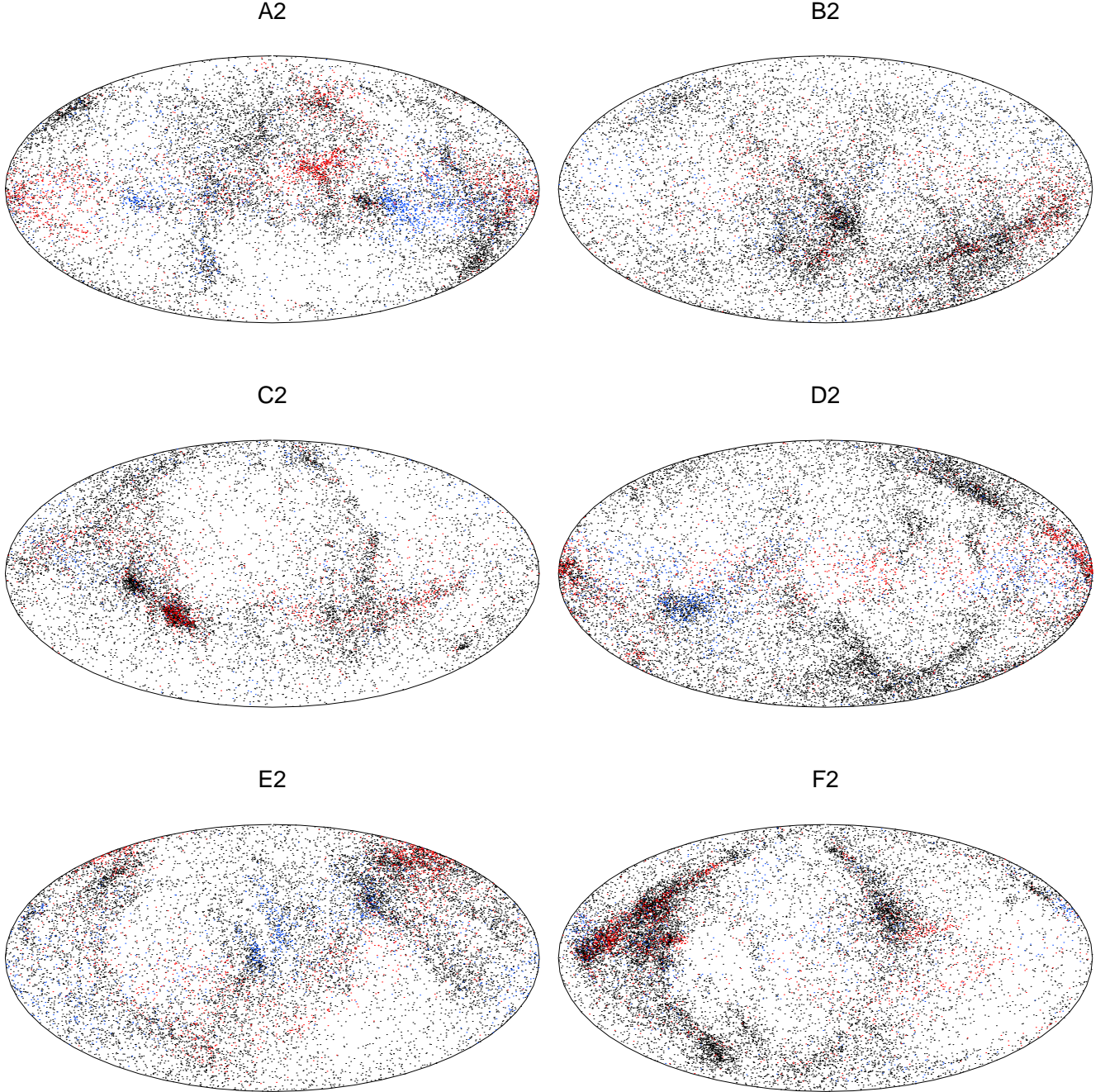


Figure 8. Mollweide projections of the position at which each subhalo enters the main halo. Subhaloes that end up in parallel spin orbits are shown in red, those that end up in antiparallel spin orbits in blue, and those with intermediate orbits in black. The main halo spin points towards the north pole of each projection. Higher quality versions of these maps are available at: <http://astro.dur.ac.uk/~d50wse/page2.html>

be present in NGC 5084 (Carignan et al. 1997) whereas a population of prograde satellites appears to be present in the Milky Way (Metz et al. 2008); Hwang & Park (2010) find equal proportions of prograde and retrograde satellites across a sample of 215 systems.

Halo Aq-A has a particularly concise formation history. This halo forms from a filament that collapses at early times and is fed by two strands at either end. A large fraction of

the subhaloes that survive to the present pass through these strands, and are propelled into either a prograde or retrograde orbit depending on the strand in which they originated. Aq-D has a similar formation history and outcome, whereas Aq-E shows that it is possible to end up with a similar orbital arrangement by a different, more complex path. Coherent rotation is exhibited by the entire population of subhaloes, not just those with the most massive progenitors

which according, for example, to Libeskind et al. (2005) are the most likely to host visible satellites.

Our analysis has implications for the expected bulk kinematics of satellite galaxies which may be probed in future galaxy surveys. We expect a variety of orbital configurations reflecting the variety of halo formation histories. Quasi-planar distributions of coherently rotating satellites should be commonplace, most rotating in the same direction as the halo (and, by implication, the main galaxy) but some in the opposite direction as found by Hwang & Park (2010).

ACKNOWLEDGEMENTS

MRL would like to thank Andrew Cooper and Owen Parry for useful discussions, and acknowledges a PhD studentship from the Science and Technologies Facilities Council (STFC). CSF acknowledges a Royal Society Wolfson Research Merit award. We thank an anonymous referee for helpful comments. This work was supported also by an STFC rolling grant to the ICC.

REFERENCES

- Allgood B., Flores R. A., Primack J. R., Kravtsov A. V., Wechsler R. H., Faltenbacher A., Bullock J. S., 2006, *MNRAS*, 367, 1781
- Bailin J., et al., 2005, *ApJ*, 627, L17
- Bailin J., Steinmetz M., 2005, *ApJ*, 627, 647
- Belokurov V., et al., 2008, *ApJ*, 686, L83
- Benson A. J., Frenk C. S., Lacey C. G., Baugh C. M., Cole S., 2002, *MNRAS*, 333, 177
- Bett P., Eke V., Frenk C. S., Jenkins A., Helly J., Navarro J., 2007, *MNRAS*, 376, 215
- Bett P., Eke V., Frenk C. S., Jenkins A., Okamoto T., 2010, *MNRAS*, 404, 1137
- Boylan-Kolchin M., Springel V., White S. D. M., Jenkins A., 2010, *MNRAS*, 406, 896
- Bullock J. S., Kravtsov A. V., Weinberg D. H., 2000, *ApJ*, 539, 517
- Busha M. T., Alvarez M. A., Wechsler R. H., Abel T., Strigari L. E., 2010, *ApJ*, 710, 408
- Carignan C., Cote S., Freeman K. C., Quinn P. J., 1997, *AJ*, 113, 1585
- Cooper A. P., et al., *MNRAS*, 406, 744
- Davis M., Efstathiou G., Frenk C. S., White S. D. M., 1985, *ApJ*, 292, 371
- Górski K. M., Hivon E., Banday A. J., Wandelt B. D., Hansen F. K., Reinecke M., Bartelmann M., 2005, *ApJ*, 622, 759
- Hoyle F., 1951, in *Problems of Cosmical Aerodynamics The Origin of the Rotations of the Galaxies*. pp 195–+
- Hwang H. S., Park C., 2010, *ApJ*, 720, 522
- Irwin M. J., et al., 2007, *ApJ*, 656, L13
- Kang X., Mao S., Gao L., Jing Y. P., 2005, *A&A*, 437, 383
- Kauffmann G., White S. D. M., Guiderdoni B., 1993, *MNRAS*, 264, 201
- Klypin A., Kravtsov A. V., Valenzuela O., Prada F., 1999, *ApJ*, 522, 82
- Koposov S. E., Yoo J., Rix H., Weinberg D. H., Macciò A. V., Escudé J. M., 2009, *ApJ*, 696, 2179
- Li Y., De Lucia G., Helmi A., 2010, *MNRAS*, 401, 2036
- Li Y., Helmi A., 2008, *MNRAS*, 385, 1365
- Libeskind N. I., Cole S., Frenk C. S., Okamoto T., Jenkins A., 2007, *MNRAS*, 374, 16
- Libeskind N. I., Frenk C. S., Cole S., Helly J. C., Jenkins A., Navarro J. F., Power C., 2005, *MNRAS*, 363, 146
- Libeskind N. I., Frenk C. S., Cole S., Jenkins A., Helly J. C., 2009, *MNRAS*, 399, 550
- Lux H., Read J. I., Lake G., 2010, *MNRAS*, 406, 2312
- Lynden-Bell D., 1976, *MNRAS*, 174, 695
- Macciò A. V., Kang X., Fontanot F., Somerville R. S., Koposov S., Monaco P., 2010, *MNRAS*, 402, 1995
- Metz M., Kroupa P., Jerjen H., 2009, *MNRAS*, 394, 2223
- Metz M., Kroupa P., Libeskind N. I., 2008, *ApJ*, 680, 287
- Moore B., Ghigna S., Governato F., Lake G., Quinn T., Stadel J., Tozzi P., 1999, *ApJ*, 524, L19
- Muñoz J. A., Madau P., Loeb A., Diemand J., 2009, *MNRAS*, 400, 1593
- Navarro J. F., et al., 2010, *MNRAS*, 402, 21
- Sakamoto T., Hasegawa T., 2006, *ApJ*, 653, L29
- Shaw L. D., Weller J., Ostriker J. P., Bode P., 2006, *ApJ*, 646, 815
- Somerville R. S., 2002, *ApJ*, 572,
- Springel V., et al., 2008b, *MNRAS*, 391, 1685
- Springel V., et al., 2008a, *Nature*, 456, 73
- Springel V., White S. D. M., Tormen G., Kauffmann G., 2001, *MNRAS*, 328, 726
- Vogelsberger M., et al., 2009, *MNRAS*, 395, 797
- Wadepuhl M., Springel V., 2011, *MNRAS*, 410, 1975
- Walsh S. M., Jerjen H., Willman B., 2007, *ApJ*, 662, L83
- Warnick K., Knebe A., 2006, *MNRAS*, 369, 1253
- White S. D. M., 1984, *ApJ*, 286, 38
- Willman B., et al., 2005, *AJ*, 129, 2692
- Willman B., et al., 2005, *ApJ*, 626, L85
- York D. G., et al., 2000, *AJ*, 120, 1579
- Zentner A. R., Kravtsov A. V., Gnedin O. Y., Klypin A. A., 2005, *ApJ*, 629, 219
- Zucker D. B., et al., 2006, *ApJ*, 650, L41
- Zucker D. B., et al., 2006, *ApJ*, 643, L103

This paper has been typeset from a \LaTeX file prepared by the author.